Title
PION STUDIES WITH SILICON DETECTORS

Authors
Raju, M.R.
Aceto, H.
Richman, C.

Publication Date
1965-04-26

UCRL-16071

University of California

Ernest O. Lawrence Radiation Laboratory

PION STUDIES WITH SILICON DETECTORS

Berkeley, California

DISCLAIMER

Submitted to Nuclear Instruments
and Methods

UCRL-16071

UNIVERSITY OF CALIFORNIA
Lawrence Radiation Laboratory
Berkeley, California

AEC Contract No. W-7405-eng-48

PION STUDIES WITH SILICON DETECTORS

M. R. Raju, H. Aceto, and C. Richman

April 26, 1965

ABSTRACT

Measurements were made of the most probable energy loss in silicon for pions of energies extending from 365 MeV to 50 MeV. The results agree within 2% with the theoretical values. The behavior of the pion beam with its inherent muon and electron contaminants, as it passes through various thicknesses of absorbing material, is displayed. Finally the energy distribution of negative pion stars in silicon is measured, and is found to be a constantly decreasing function with increasing energy, with the high-energy tail extending beyond 60 MeV.

UCRL-16071

PION STUDIES WITH SILICON DETECTORS

M. R. Raju, H. Aceto, and C. Richman*

Donner Laboratory and Donner Pavilion
Lawrence Radiation Laboratory
University of California
Berkeley, California

April 26, 1965

1. Introduction

This study was initiated because of recent interest in negative pions for therapeutic applications[1-4]. When a negative pion is brought to rest in a medium, say tissue, it may be captured by a constituent nuclei, resulting in "star" events. In such interactions about 20% of the total rest energy of the π^- meson, that is, approximately 30 MeV, appears in the form of α particles and protons with ranges less than 1 mm in biological tissue[2]. It is very important to know the energy distribution of this pion star. Some measurements of the energy of these star fragments have been made using a diffusion cloud chamber[5] and emulsions[6]. Semiconductor detectors are used in the present investigation to look at the pion beam passing through various thicknesses of absorbing material and finally to measure the energy distribution of negative pion stars in silicon.

Until recently it was not possible to use semiconductor detectors for detecting particles producing a very small ionization, such as γ rays or very fast particles because the ionization was near minimum. This limitation is due to the fact that these detectors had only a very small thickness. Now the technology has been improved and detectors several mm thick are available (see reference 7 for example).

*Graduate Research Center of the Southwest, Dallas, Texas.

Semiconductor detectors have been extensively used for the detection of low-energy particles[8]. There have been very few studies relating the application of these detectors to detecting high-energy particles at the minimum-ionizing region. Miller et al.[9] could observe a good peak for 750-MeV/c π^- by using a silicon p-n junction detector. In addition, they could differentiate a mixture of positive pions and protons of 750 MeV/c momentum. The resolution they obtained for the detection of these high-energy particles is of the order of approximately 34%, which is in reasonable agreement with the Landau effect. Van Putten et al.[10] determined the most probable energy loss and energy-loss distribution of negative pions at 1.50 and 2.55 BeV/c, using a gold-doped silicon crystal. The results confirmed the density effect as described by Sternheimer[11]. Koch et al.[12] measured the most probable energy loss of relativistic mesons and protons (0.5 to 1.5 BeV/c) as a function of momentum for silicon.

In practice a π^--meson beam contains an appreciable contamination of μ mesons and electrons. Lithium-drifted silicon detectors made as described by Goulding and Hansen[13] were employed here to analyze the composite beam, both directly and after being degraded by absorbers. Measurements were made for both positive and negative pions. The measurements of most probable energy-loss for pions in silicon were made and compared with predicted values. Finally, sufficient Lucite absorber thickness was used to degrade the beam so that a substantial number of pions stopped in the silicon detector. The detector was then used to measure the energy distribution of π^- stars in silicon.

2. Calibration

The experimental setup is shown in fig. 1. The test pulse generator is used to simulate detector pulses and to check the linearity of the electronic system.

An Am^{241} alpha source and a Bi^{207} internal-conversion electron source are used for calibrating the pulse-generator output in terms of energy. Calibration and linearity checks are made for every experiment.

The Berkeley heavy-ion linear accelerator (Hilac) accelerates nuclei to an energy of 10.38 MeV per nucleon. For helium nuclei the energy of the primary beam is 41.52 MeV. The beam comes out through a vacuum column with a 1-mil aluminum window. The detector is enclosed by a housing (in order that a vacuum can be maintained) with a 1-mil Mylar window. The entire detector-holder assembly is surrounded with a 1/4-mil aluminum electronic shield. By applying the correction for the degradation of the energy of the primary beam through these foils, the energy of the primary beam seen by the detector is found to be 40 MeV. A typical spectrum produced by totally absorbed α particles is shown in fig. 2. In a detector where a particle is stopped, the resolution is a function of the detector and the electronic system. Values for full width at half maximum from 2 keV upwards (depending upon the type of experiment) have been obtained by many workers with semiconductor detectors exposed to monoenergetic particles, giving resolutions much less than 1%. Full width at half maximum obtained in this measurement if 0.62 MeV, giving a resolution of 1.5% (when the detector is operated at room temperature). This poorer resolution is partly due to momentum spread of the beam and partly due to noise in the amplifier. However, better resolutions can be obtained by operating the detector at low temperature and using better amplifiers.

The energy of the beam based upon the earlier calibration is 39.88 MeV, which agrees very well with the primary energy of 40 MeV. This agreement confirms the calibration and linearity of the system up to 40 MeV. Further experiments with α particles confirm the linearity of the system up to an investigated energy of 85 MeV.

3. Determination of Detector Thickness

The thickness of the detector depletion layer determines the energy loss for particles passing completely through the detector. In our case, the depletion layer extends almost through the entire physical thickness of the detector except for a few mils on the Li side. The method used to measure this depletion thickness is to determine the maximum energy deposited in the detector. The range of the α particle whose energy corresponds to this maximum energy is then obtained from range-energy tables[14]. The 910-MeV alpha beam is degraded so that the energy of the emergent beam is close to the energy corresponding to the range of the alpha beam in the detector. The response of the two detectors used in the present investigations for a degraded primary beam of 910-MeV α particles is shown in figs. 3 and 4.

For α particles whose range is greater than the depth of the depletion region, the charge-pulse amplitude from the detector increases with decreasing alpha energy until the energy corresponds to the depletion thickness of the detector. A further decrease in alpha energy will cause a proportional decrease in charge pulse. It can be seen from figs. 3 and 4 that the maximum cutoff energy for the two detectors used (corresponding to the range in the detector) is 70 and 83 MeV, respectively. The corresponding ranges from range-energy tables are 0.45 and 0.61 g/cm^2 respectively.[14]. The physical thicknesses of the detectors as

determined with a micrometer are 6% greater than these values. This difference is due to the dead layer on the Li side. The experimental accuracy in the determination of detector thickness is within about 2%.

4. Production of Negative and Positive Pions

The Berkeley 184-inch synchrocyclotron produces an intense beam of 732-MeV protons, and in their outer orbit they strike a 2-in.-thick beryllium target. When these protons collide with beryllium nuclei, π^0, π^+, and π^- mesons are produced. The experimental arrangement for π^- is shown in fig. 5. To get a π^+ beam, all the magnetic fields are reversed, including that of the cyclotron. The magnetic lens system remains unchanged for pions of the same energy. The bending magnet removes particles of different Hρ than the pions that are being used. The cyclotron produces pions in a range of energies of hundreds of MeV. In our experiments, we used π^- of 370 MeV and both π^+ and π^- of 95 MeV.

The cyclotron pulses 64 times per second, thus giving 64 coarse groups of pions per second. The mode of operation can be controlled so that these groups of pions can be spread out over either of two periods of time. The "short spill" mode spills the beam over a period of approximately 400 μsec. The auxiliary dee mechanism of the cyclotron makes it possible to spread each group of pions over a longer period of 8 msec. The long-spill operation results in a cyclotron duty cycle of about 51%, compared with 2.5% for the short spill. Long-spill operation is used throughout the experiment. Hence, for the detector exposed to pions at rates of about 10^3/sec, accidental counting loss should be negligible.

5. Experimental Results of $\frac{dE}{dX}$ Measurements

5.1. 365-MeV π^- Beam

Pion beams are always produced with muon and electron contamination. Depending on the energy of the pion beam and the focusing setup, the relative percentage of muons and electrons with respect to pions varies[15]. The percentage contamination varies inversely with energy, and at 365 MeV the percentage contamination of muons and electrons is very small.

Figure 6 shows the detector response obtained with 365-MeV π^- mesons. These pions are close to the minimum-ionizing region. There is a distinct pion peak whose corresponding energy is close to the theoretically predicted value. The resolution is about 33%, which is in reasonable agreement with the Landau effect. As we increased the thickness of the copper absorber in the beam, the energy of the pion would be lowered and hence the dE/dx would increase, with a concomitant increase in the energy spread. The experimental and theoretical values are in close agreement down to a residual energy of 164 MeV. At lower energies this agreement is lacking, because of the uncertainty of the determination of residual energy which results from the constant increase in energy spread.

The experimental values of energy loss in the 0.45-g/cm^2-thick silicon detector, compared to the theoretical values as calculated using the Landau approximation, are shown in Table I. The residual energies of the degraded beam are determined by using the range-energy tables of Rich and Madey[17].

5.2 95-MeV π^+ Beam

Figure 7 shows the result obtained with a 95-MeV π^+ beam whose muon and positron contamination is very small. Figures 8 through 10 show the same beam degraded by various thicknesses of Lucite. A number of features of these data are interesting.

First, the resolution is in reasonable agreement with the Landau effect. Secondly, the peaks are shifted to higher energies as the thickness of the Lucite absorber is increased. Very interesting things are observed close to the end of the range. Figure 8 shows the response of the detector for a 95-MeV π^+ beam degraded with 7.5 in. of Lucite. This thickness of Lucite is 1 in. less than the range of these pions. A small peak at 1.15 MeV is noticed in addition to the 1.98-MeV π^+ peak. This small peak is due to μ^+ particles formed by the decay of π^+ mesons. Figure 9 shows the response of the detector for the beam degraded by 8.5 in. of Lucite, which corresponds to the Bragg peak position. Both the muon and pion peaks are shifted to higher energies. At 10 in. of Lucite (which is beyond the range of pions), the pion peak has disappeared and the peaks due to positrons at 0.87 MeV and muons at 1.32 MeV remain. At 9.5 in. of Lucite plus 3/8 in. copper (because of the lack of space, copper is used to substitute for an equivalent thickness of Lucite), which is beyond the range of pions and muons, only the electron peak at 0.92 MeV is observed, as shown in Fig. 10.

5.3 95-MeV π^- Beam

Unlike the other two beams, this beam is contaminated with approximately 25% electrons and approximately 10% muons. Figure 11 shows the response of the 95-MeV (189-MeV/c) negative pion beam, including its muon and electron contamination. Two peaks at 0.87 and 1.05 MeV are

clearly visible. They are due to electrons and pions, respectively. The muon contamination, being relatively small, is hidden in the distribution of electrons and pions. Figures 12 through 15 show the response of the detector for various thicknesses of Lucite introduced in the beam. It can be noticed that as the absorber thickness increases, the relative height of the pion peak decreases in comparison with the electron peak. This result is due to a higher nuclear collision cross section of pions in comparison with electrons. The results obtained with a time-of-flight system confirms this behavior. As the thickness of Lucite increases, the peak due to electrons remains at the position corresponding to about 0.87 MeV, while the peak due to pions shifts to higher energies. This is because the electrons of initial momentum 189 MeV/c are still in the minimum-ionizing region, while the pion energy losses change considerably as the thickness of Lucite absorber increases. Beyond the range of pions (i.e., for thicknesses greater than 8-5/8 in. of Lucite), the pion peak is absent and the electron peak persists.

The experimental values of the most probable energy losses of pions (both positive and negative) are given along with theoretical values in Table II. Since for lower energies the Landau approximation breaks down at large detector thicknesses, probable energy loss must be computed by using the rigorous Vavilov expression[18] as tabulated by Seltzer and Berger[19]. Values obtained by using the Landau approximation in this particular case would be about 3% higher than those obtained by using the Vavilov expression. The residual energy of the pion beam after passing through various thicknesses of Lucite absorbers is computed from range-energy tables[17].

The agreement between the Vavilov-derived values and the experimental values is within 2% down to a residual energy of 44 MeV (corresponding

to a Lucite absorber thickness of 6 in.). At lower energies the agreement is very poor, as noted for 365-MeV π^-.

6. Measurement of the Energy Distribution of Pion-Produced Stars in Silicon

We obtained the Bragg curve for the pion beam with the argon-CO_2-filled ionization chambers in the classical fashion, using one chamber as a monitor followed by different thicknesses of Lucite absorber and then using the second ionization chamber as a detector. For this beam the Bragg peak is obtained at 8-5/8 in. of Lucite absorber. Most of the pions stop in this region and create stars. The width of the Bragg peak at 50% level is approximately 1.89 g/cm^2 of Lucite.

The thickness of the semiconductor used in this study is 0.61 g/cm^2. Hence, if the detector were sitting at the Bragg peak position, a good portion of the pions would be stopped in the detector and create stars in silicon. In addition to the energy of stars formed in the detector because of pions stopped there, the detector at this position would also see the energy loss of the pions, muons, and electrons passing through the detector.

In order for the detector to see the energy distribution of the pion star alone, the energy deposited by the pions, muons, and electrons while passing through the detector has to be eliminated. This is achieved by using another semiconductor detector in anticoincidence with the analyzing detector. The schematic diagram is shown in fig. 1. In this way we can observe only the pions that stop in the analyzing detector (i.e., pion stars), and the rest of the events can be eliminated. However, sometimes one of the prongs of the stars in the first detector can pass through the second detector and cause anticoincidence, thereby losing some stars. This does

not greatly affect the energy distribution of the pion stars. Figure 16 shows the energy distribution of the pion stars. The upper curve shows the distribution without using the second detector in anticoincidence, so that the detector sees, besides the energy of the stars, quite a few low-energy events due to pions, muons, and electrons passing through the detector. The bottom curve is obtained by using the anticoincidence detector, thereby giving the energy distribution of pion stars in silicon.

The thickness of the detector corresponds to the range of approximately 84-MeV α particles and 20-MeV protons. Therefore this energy distribution of pion stars does not correspond to the total energy of the star, but only to that fraction of the energy of the star fragments that is deposited in the detector. Most of the α-particle energy and that from heavier fragments would be stopped in the detector. Indeed, this is also true for the protons with the exception that some of the higher-energy protons may escape the detector, depositing only a fraction of their energy. On the other hand, neutrons would escape the detector most of the time. It can be seen from fig. 16 that the number of stars is a constantly decreasing function with increasing energy and that this star energy extends beyond 60 MeV. Since both the curves are for the same amount of charge collected in the monitor chamber, strictly speaking they should both coincide up to about 10 MeV. However, the lower curve (for the anticoincidence detector) is less than the upper curve (for a single detector), thereby indicating that some of the star events are lost when the anticoincidence detector is used, because some of the fragments pass through the analyzing detector and reach the anticoincidence detector.

Acknowledgments

We wish to thank Professor John H. Lawrence and Professor Cornelius A. Tobias for their continued interest and encouragement. Special thanks to D. Landis, R. Lathrop and H. Smith for supplying the detectors and helpful discussions on their use. Also, the discussions with Fred Goulding in preparation of this paper are most appreciated. Finally, we wish to thank Mr. Howard Maccabee for making the theoretical calculations. This work was done under the auspices of the U. S. Atomic Energy Commission. **and the American Cancer Society.**

1) C. Richman, (Lawrence Radiation Laboratory), unpublished data, 1952.

2) R. H. Fowler, and D. H. Perkins, Nature, 189 (1961) 524.

3) C. Richman, H. Aceto, Jr., M. R. Raju, B. Schwartz, and M. Weissbluth, On the Dosimetry of Negative Pions with a View Toward Their Trial in Cancer Therapy, in Biology and Medicine Semiannual Report, Lawrence Radiation Laboratory Report UCRL-11387, Spring 1964 (unpublished).

4) C. Richman, H. Aceto, Jr., M. R. Raju, and B. Schwartz, The Therapeutic Possibilities of Negative Pions--Preliminary Physical Experiments, submitted to Am. J. Roentgenology, Radium Therapy and Nuclear Medicine.

5) P. Ammiraju, and L. M. Lederman, Nuovo Cimento, 4 (1956) 283.

6) M. G. K. Menon, H. Muirhead, and O. Rochat, Phil. Mag., 41 (1950) 583.

7. Conclusions

The lithium-drifted silicon semiconductor detectors used in this study give very promising results in measuring energy loss of high-energy particles. Indeed, the agreement between the theoretical and experimental values of energy loss is within 2%. The behavior of the pion beam as it passes through various thicknesses of absorbing material is dramatically displayed with instrumentation that is relatively simple when compared with other instrumentation used with high-energy machines. The composite beam of pions, muons, and electrons of the same momentum can be differentiated.

The pion star energy spectrum is a constantly decreasing function with increasing energy, with the high-energy tail extending beyond 60 MeV. An attractive feature of these detectors is that they operate as true energy-measuring devices in that they do not exhibit the saturation effects of scintillator counters.

7) F. Goulding, A Survey of the Applications and Limitations of Various Types of Detectors in Radiation Energy Measurements, in Physics Division Semiannual Report, Lawrence Radiation Laboratory Report UCRL-11132, Feb. 1964 (unpublished).

8) Solid State Radiation Detectors, in IRE Trans. Nucl. Sci. 8 (Jan. 1961).

9) Ibid., p. 73.

10) Ibid., p. 124.

11) R. M. Sternheimer, Phys. Rev., 115 (1959) 137.

12) L. Koch, J. Messier, and J. Valin, Nuclear Electronics, (I.A.E.A., Vienna, 1962) 1, 465.

13) F. G. Goulding, and W. L. Hansen, IEEE Trans. Nucl. Sci., (1964), 286.

14) L. Williamson, and J. P. Boujot, Tables of Range and Rate of Energy Loss of Charged Particles of Energy 0.5 to 150 MeV, 1962.

15) A. Astbury, K. M. Crowe, J. G. Deutsch, Tin Maung, and R. E. Taylor, Study of Optimum Target Positions for the Secondary Meson Beams from the 184-inch Cyclotron, Lawrence Radiation Laboratory Report UCRL-10120, March 1962 (unpublished).

16) L. Landau, Zh. Eksperim. i Teor. Fiz., 8 (1944) 201.

17) M. Rich, and R. Madey, Range-Energy Tables, University of California Radiation Laboratory Report UCRL-2301, March 1954 (unpublished).

18) P. N. Vavilov, Zh. Experim. i Teor. Fiz., 32, (1957) 320
English Transl: Soviet Phys. --JETP 5 (1957) 749.

19) S. M. Seltzer, and M. J. Berger, "Energy Loss Straggling of Protons and Mesons: Tabulation of the Vavilov Distribution," in Studies in Penetration of Charged Particles in Matter, NAS-NRC Pub. #1133 (1964), p. 187.

Table I. 365-MeV π^- Beam in 0.45-g/cm^2 silicon detector

Thickness of copper absorber (in.)	Residual energy (MeV)	Energy loss (MeV)	
		Theory	Experiment
0	365	0.596	0.60
2	295	0.602	0.60
4	230	0.616	0.63
6	164	0.660	0.66
8	92	0.794	0.82

Table II. 95-MeV π Beam in 0.61 g/cm^2 Si detector

Thickness of Lucite absorber (in.)	Residual energy (MeV)	Theoretical energy loss (MeV)		Experimental energy loss (MeV)	
		Landau	Vavilov	π^+	π^-
0	95	1.08	1.05	1.07	1.05
2	80	1.17	1.13	1.13	1.12
3	72	1.23	1.19		1.18
4	63	1.32	1.28	1.28	1.28
5	54	1.45	1.40		1.35
6	44	1.61	1.56	1.55	1.54
7	34	1.93	1.87		1.92
8	18	3.20	3.21		2.40

Figure Legends

Fig. 1. Experimental setup.

Fig. 2. Spectrum of Hilac α beam.

Fig. 3. α Spectrum for detector used with 365-MeV π^- beam.

Fig. 4. α Spectrum for detector used with 95-MeV $\pi^\pm$ beam.

Fig. 5. π-Meson experimental arrangement.

Fig. 6. Detector response to 365-MeV π^- beam.

Fig. 7. Detector response to 95-MeV π^+ beam.

Fig. 8. Detector response to 95-MeV π^+ beam degraded by 7.5 in. of Lucite.

Fig. 9. Detector response to 95-MeV π^+ beam degraded by 8.5 in. of Lucite.

Fig. 10. Detector response to 95-MeV π^+ beam degraded by 9.5 in. of Lucite and 3/8 in. of copper.

Fig. 11. Detector response to 95-MeV π^- beam.

Fig. 12. Detector response to 95-MeV π^- beam degraded by 3 in. of Lucite.

Fig. 13. Detector response to 95-MeV π^- beam degraded by 5 in. of Lucite.

Fig. 14. Detector response to 95-MeV π^- beam degraded by 8 in. of Lucite.

Fig. 15. Detector response to 95-MeV π^- beam degraded by 10 in. of Lucite.

Fig. 16. Energy distribution of pion stars.

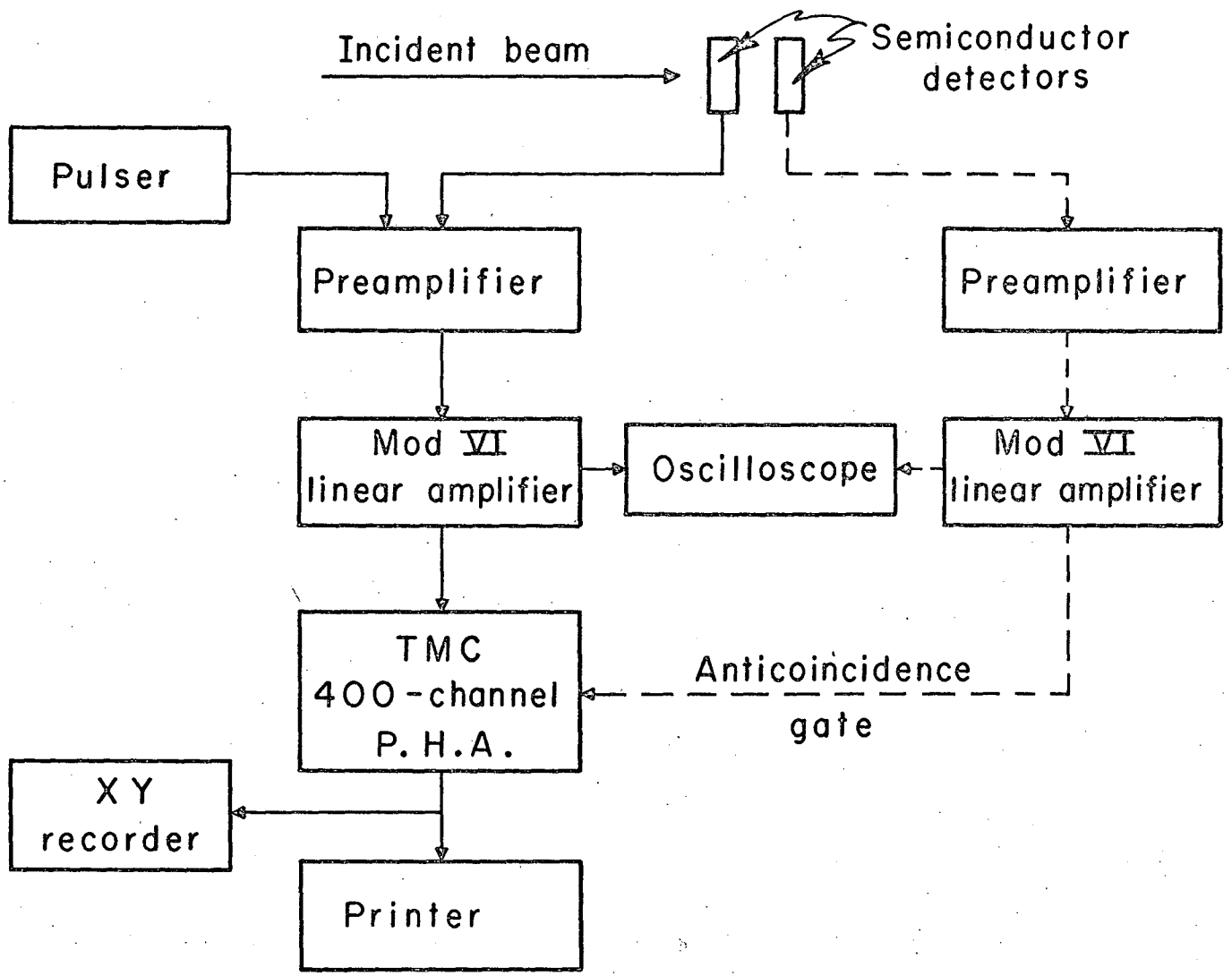

Fig. 1 MUB-4136

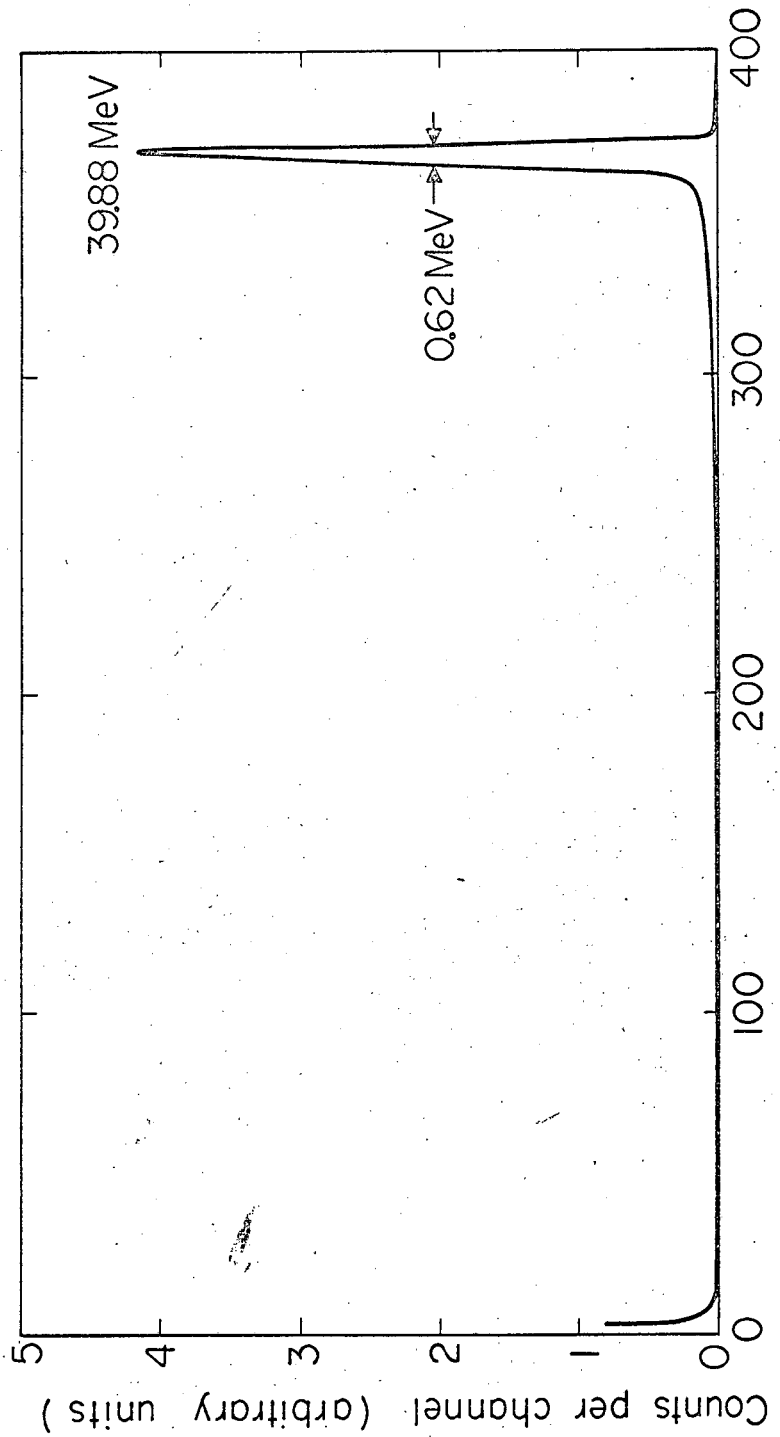
39.88 MeV
0.62 MeV
Counts per channel (arbitrary units)
Channel number
0
1
2
3
4
5
100
200
300
400
MUB-6093

Fig. 2

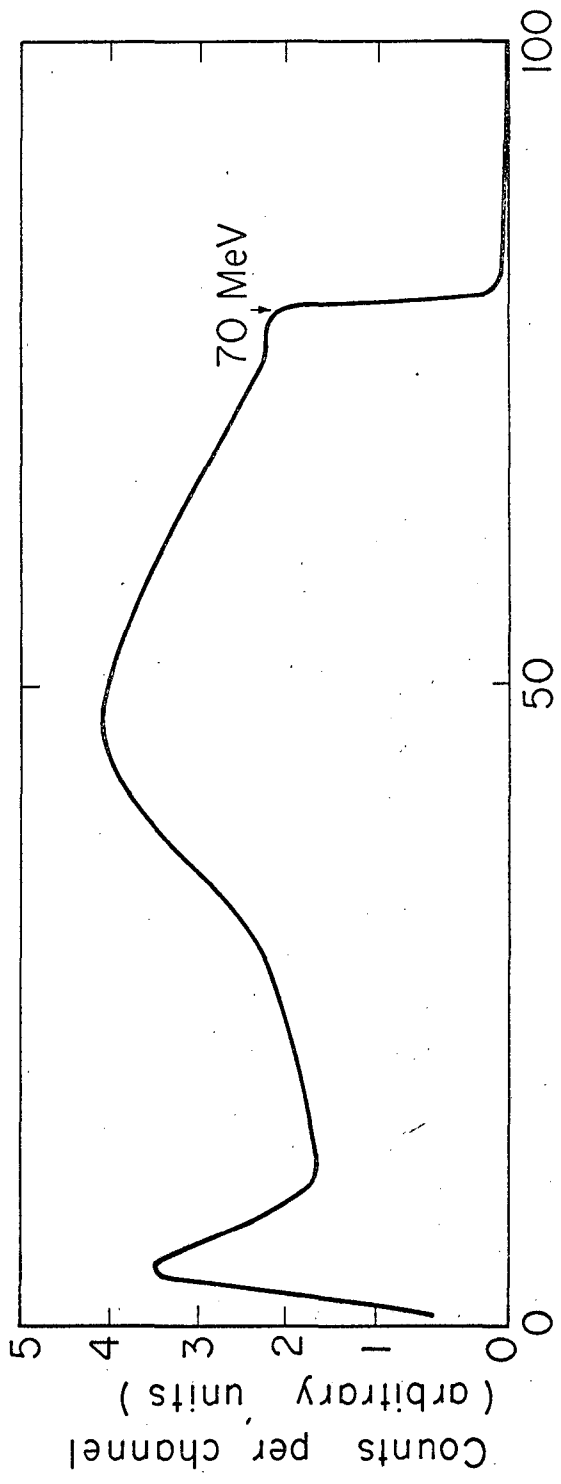
Counts per channel
(arbitrary units)
0
1
2
3
4
5
0
50
100
Channel number
70 MeV
MUB-6092

Fig. 3

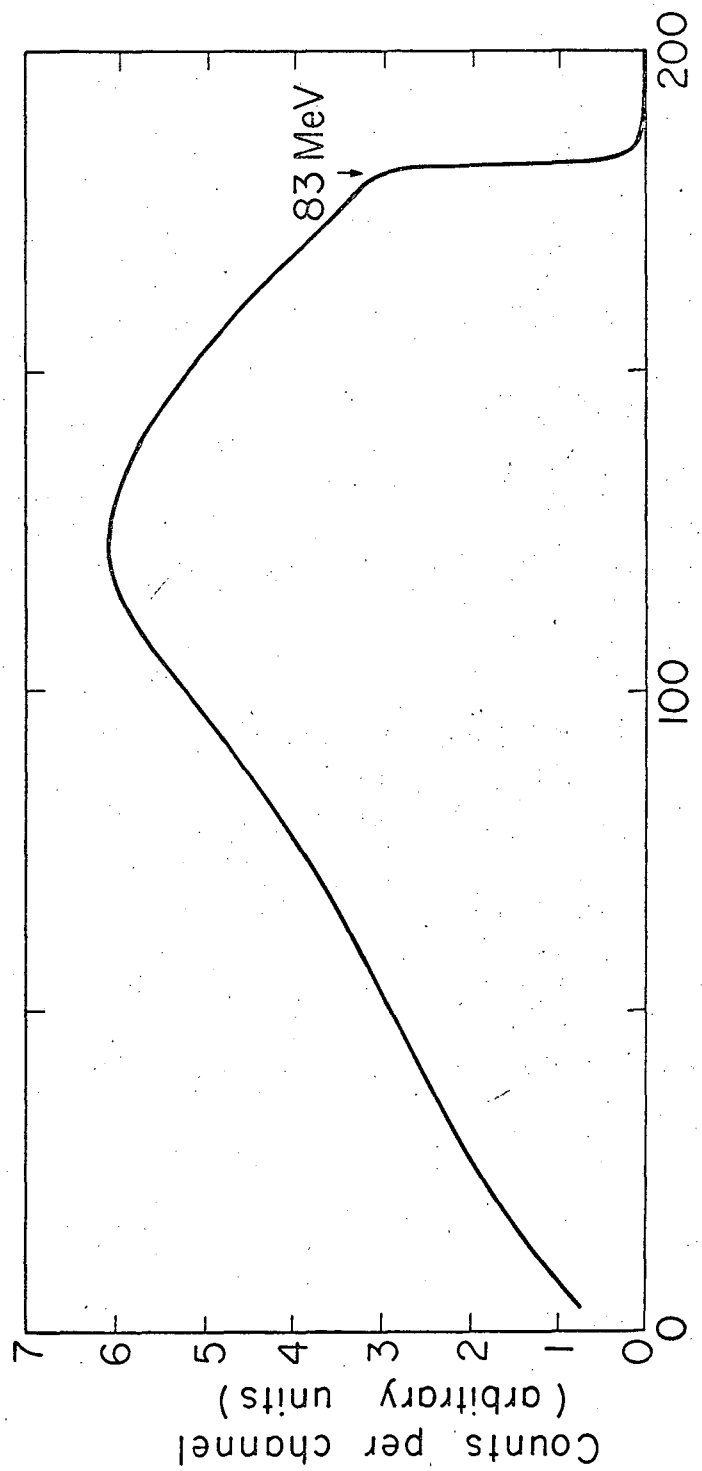
83 MeV
0
100
200
Channel number
0
1
2
3
4
5
6
7
Counts per channel
(arbitrary units)
MUB-6091

Fig. 4

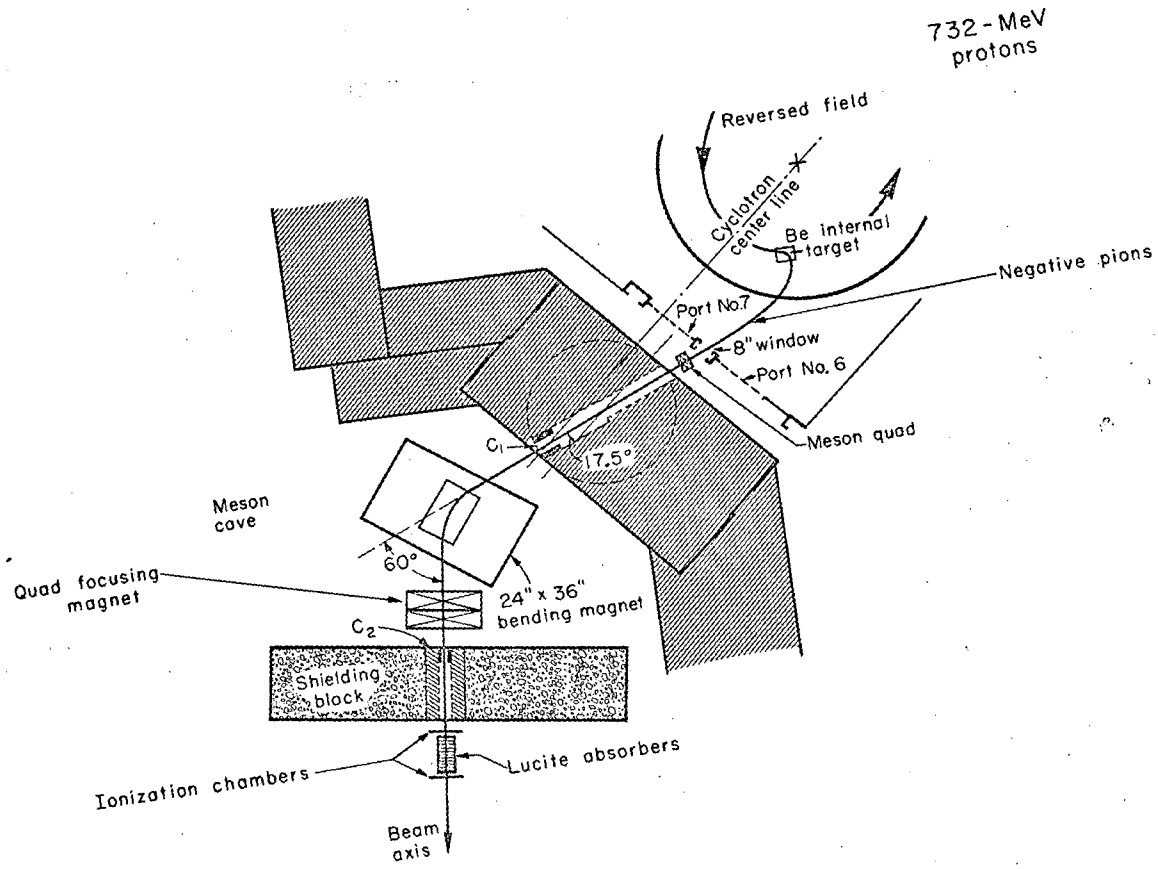
732-MeV
protons
Reversed field
Cyclotron
center line
Be internal
target
Negative pions
Port No.7
8" window
Port No. 6
Meson quad
17.5°
C_1
Meson
cave
60°
Quad focusing
magnet
24" x 36"
bending magnet
C_2
Shielding
block
Ionization chambers
Lucite absorbers
Beam
axis
MUB-966

Fig. 5

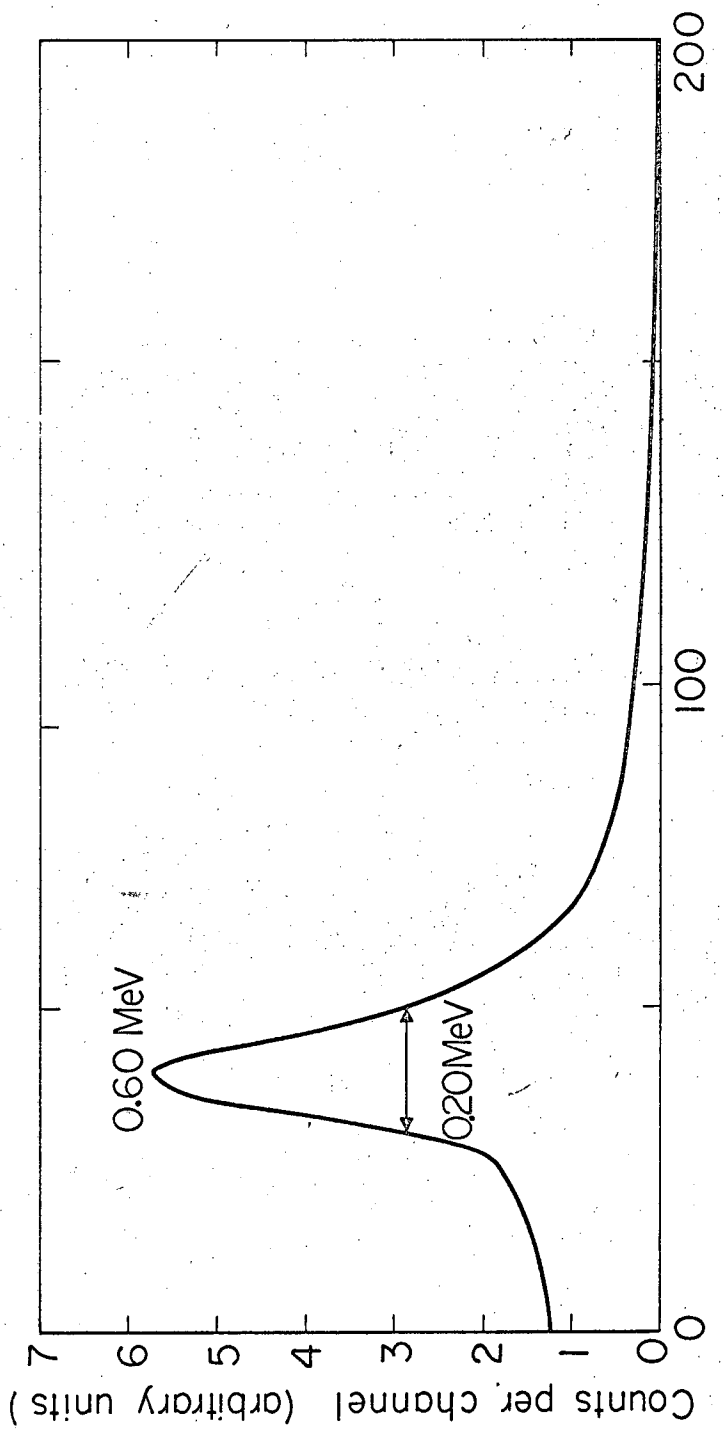
Counts per channel (arbitrary units)
0
1
2
3
4
5
6
7
0
100
200
Channel number
0.60 MeV
0.20MeV
MUB-6094

Fig. 6

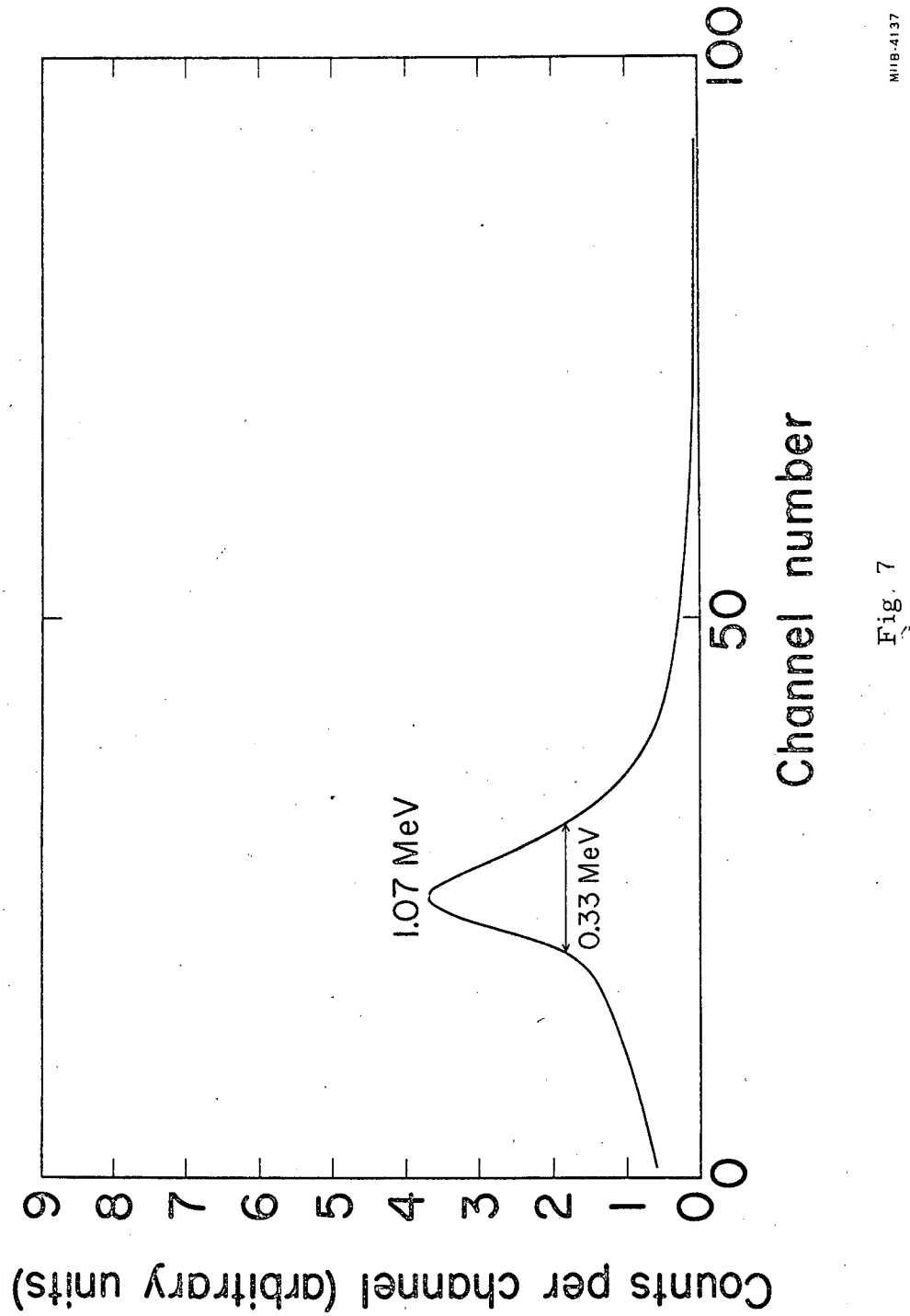
Counts per channel (arbitrary units)
0
1
2
3
4
5
6
7
8
9
0
50
100
Channel number
1.07 MeV
0.33 MeV
MUB-4137

Fig. 7

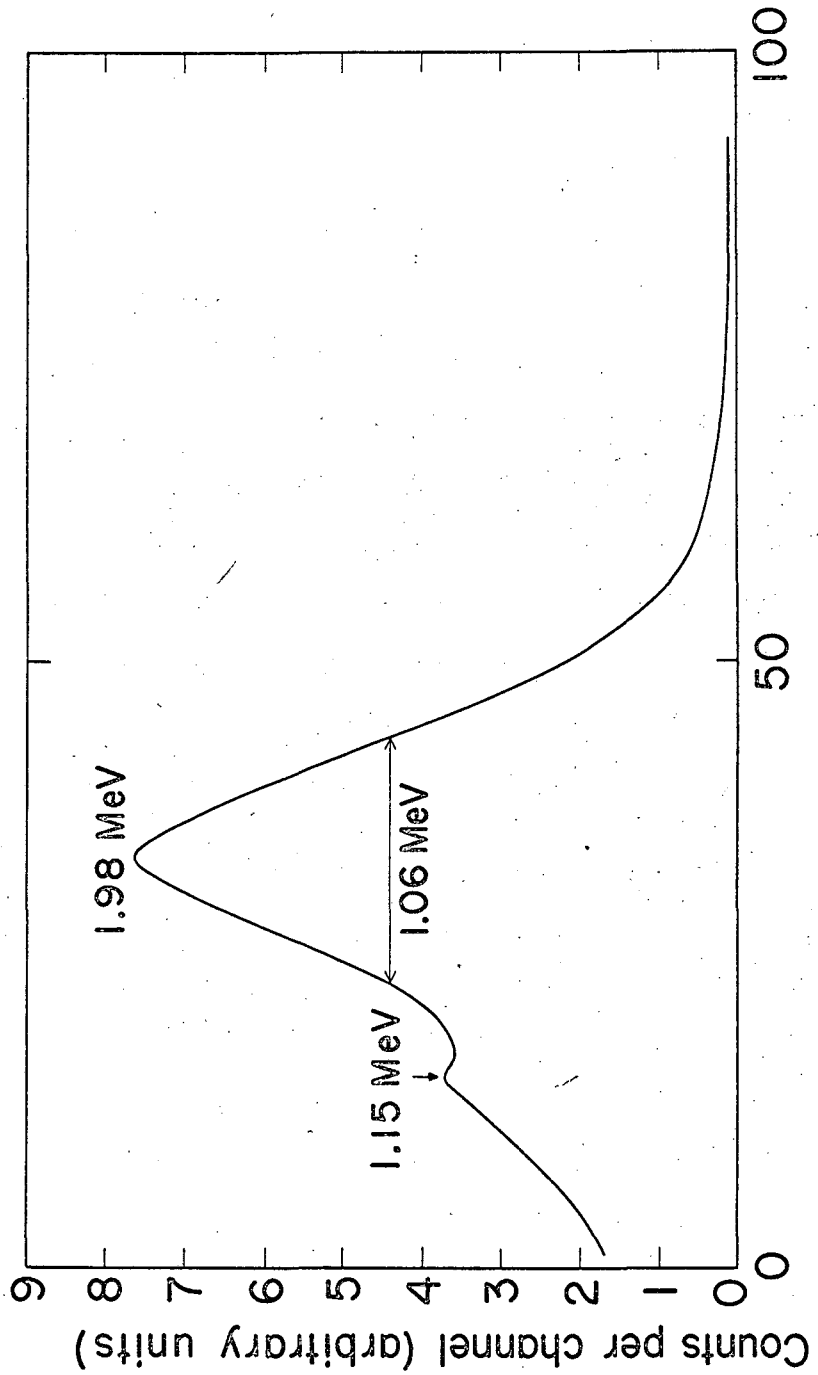
Counts per channel (arbitrary units)
0
1
2
3
4
5
6
7
8
9
0
50
100
Channel number
1.98 MeV
1.06 MeV
1.15 MeV
MUB-4140

Fig. 8

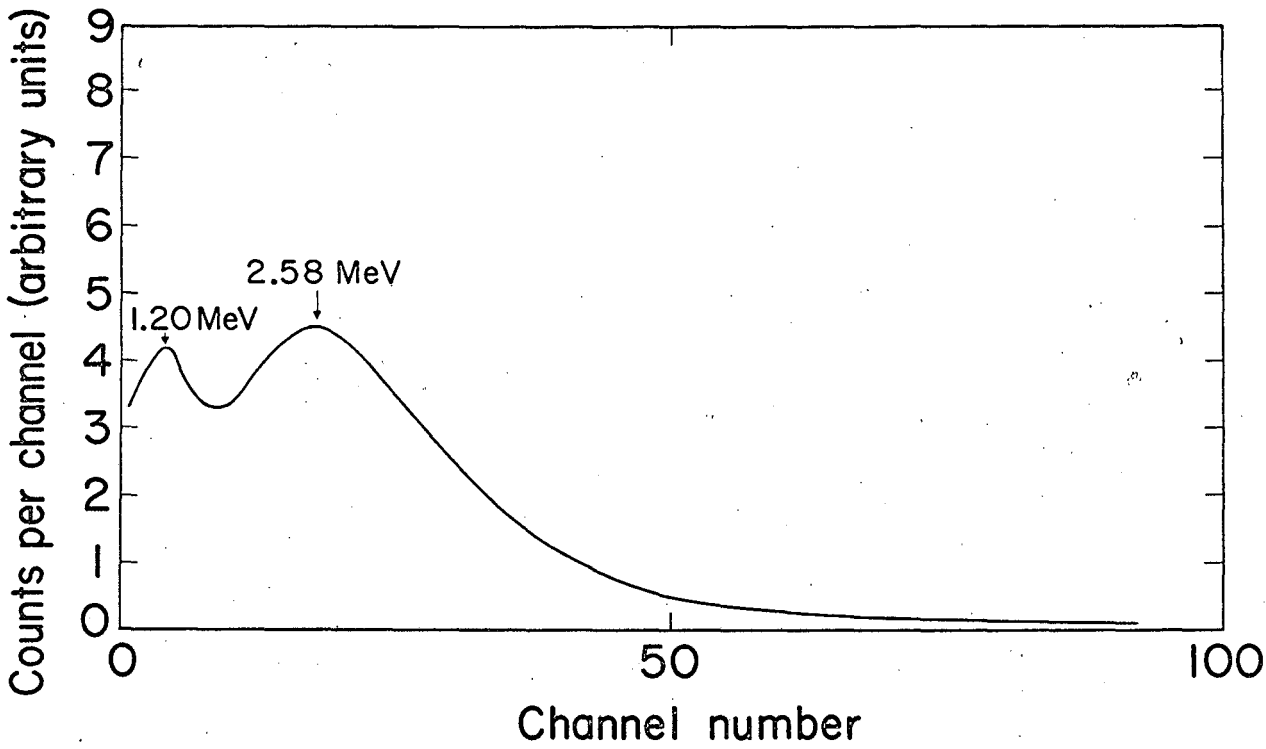
Counts per channel (arbitrary units)
0
1
2
3
4
5
6
7
8
9
1.20 MeV
2.58 MeV
0
50
100
Channel number
MUB-4141

Fig. 9

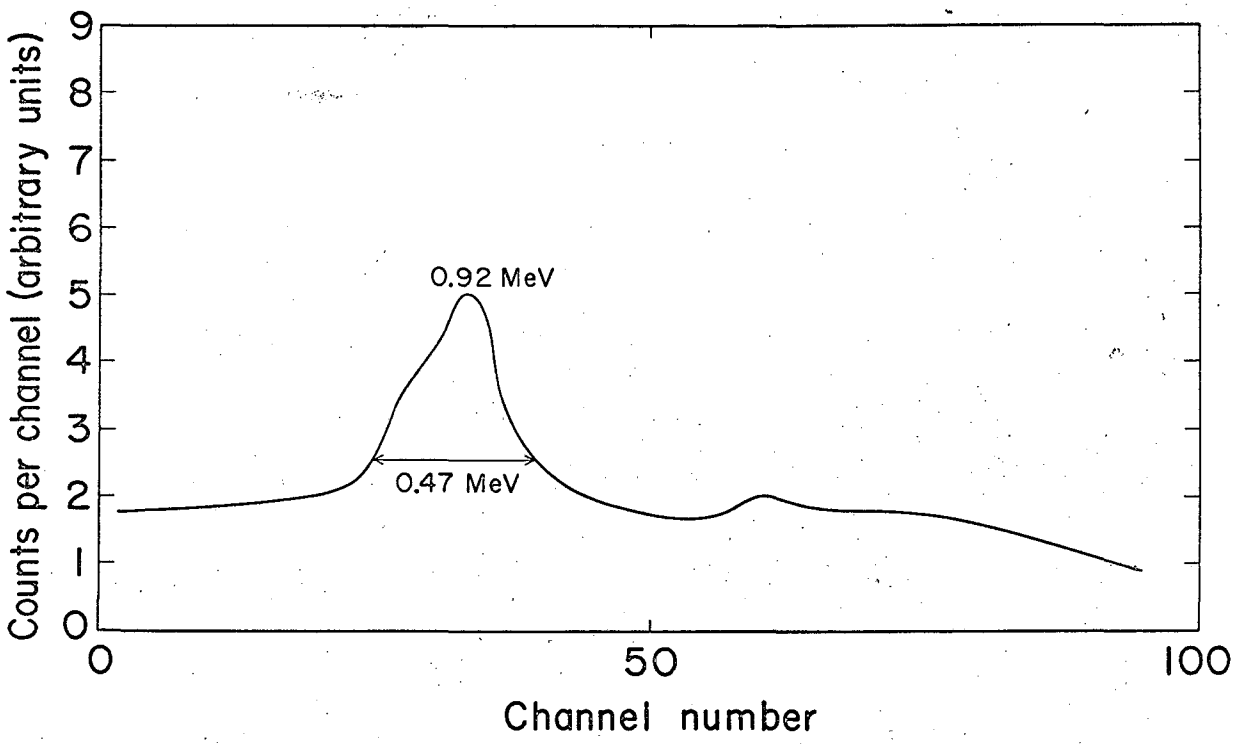
Counts per channel (arbitrary units)
0
1
2
3
4
5
6
7
8
9
0.92 MeV
0.47 MeV
0
50
100
Channel number
MUB-4142

Fig. 10

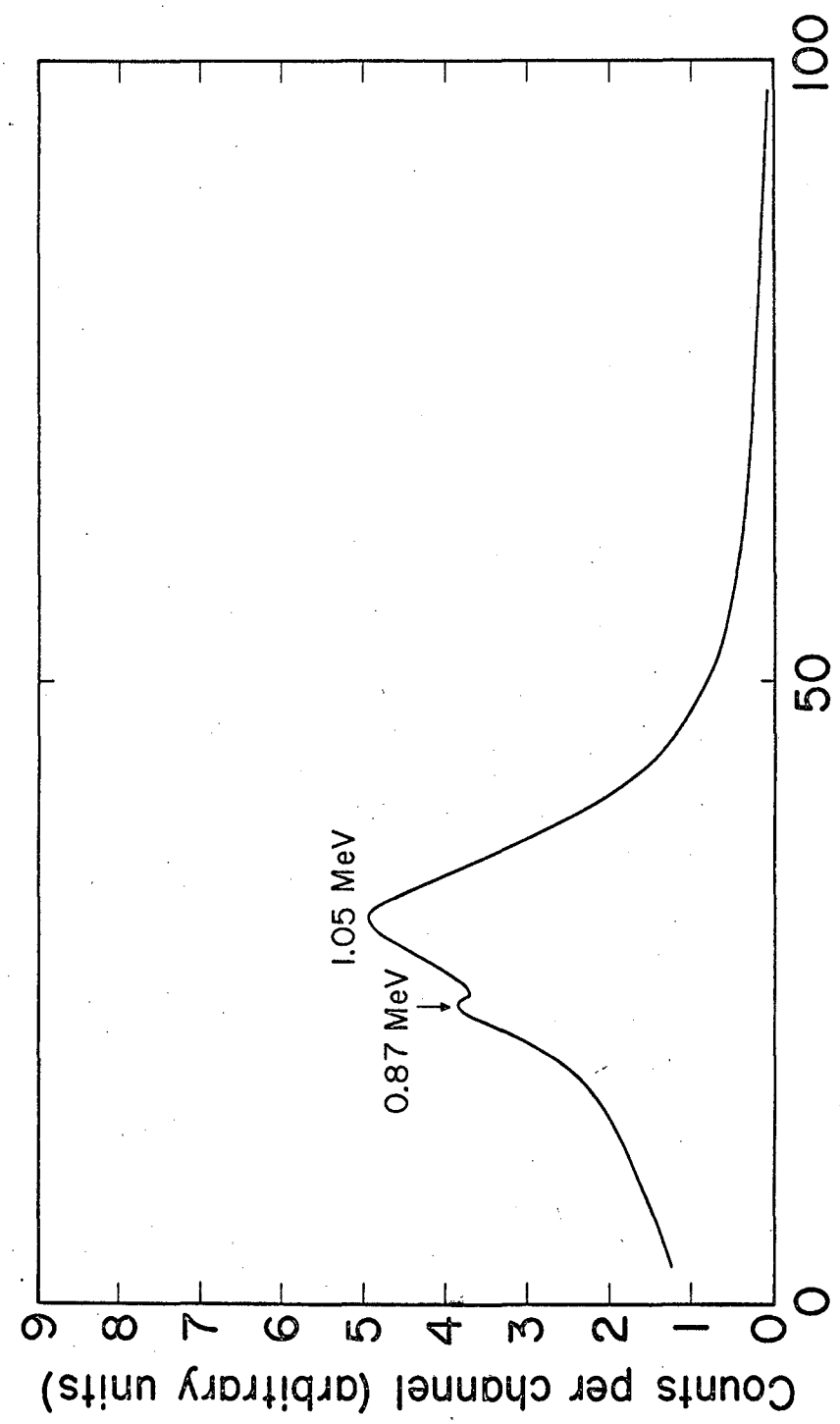
Counts per channel (arbitrary units)
0
1
2
3
4
5
6
7
8
9
0
50
100
Channel number
1.05 MeV
0.87 MeV
MUB-4138-A

Fig. 11

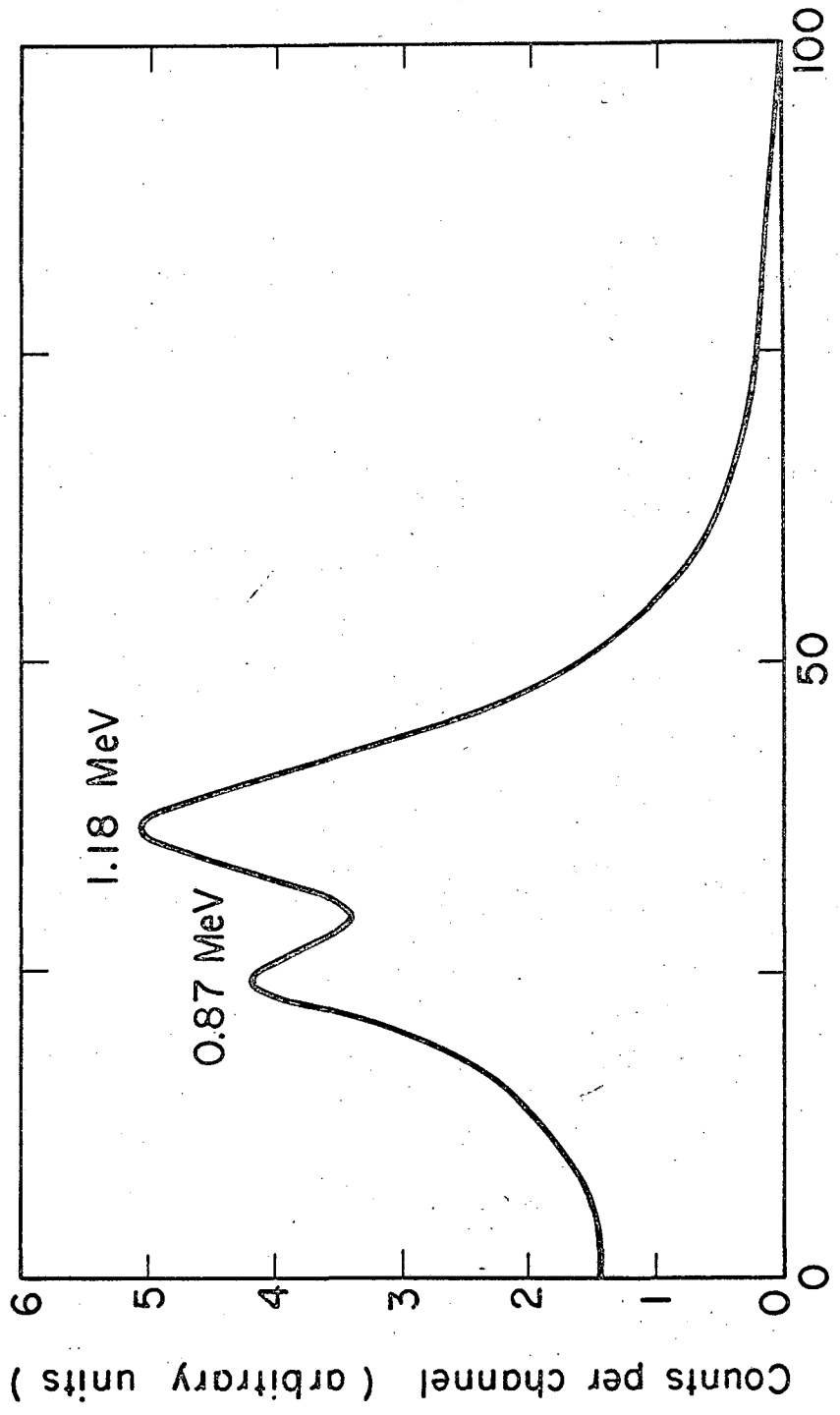

MUB-6089

Fig. 12

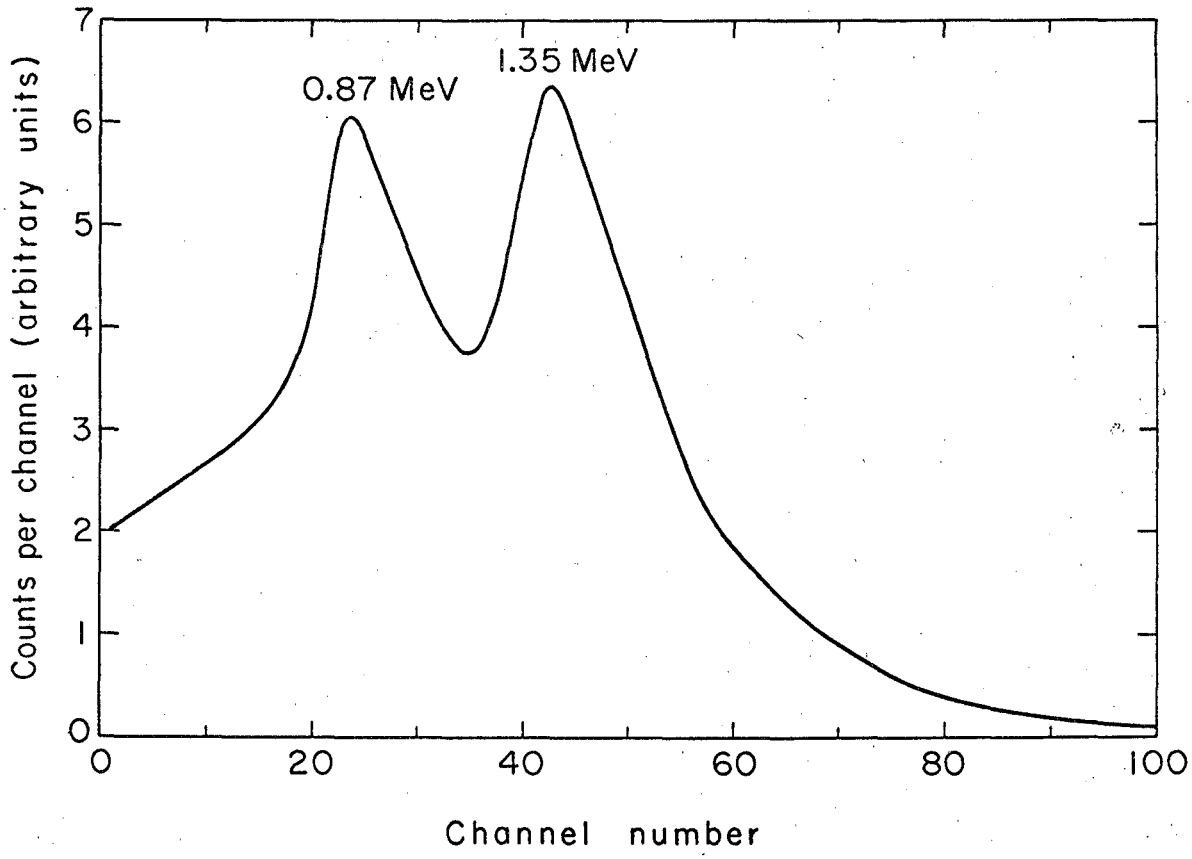

Fig. 13

MUB-4135

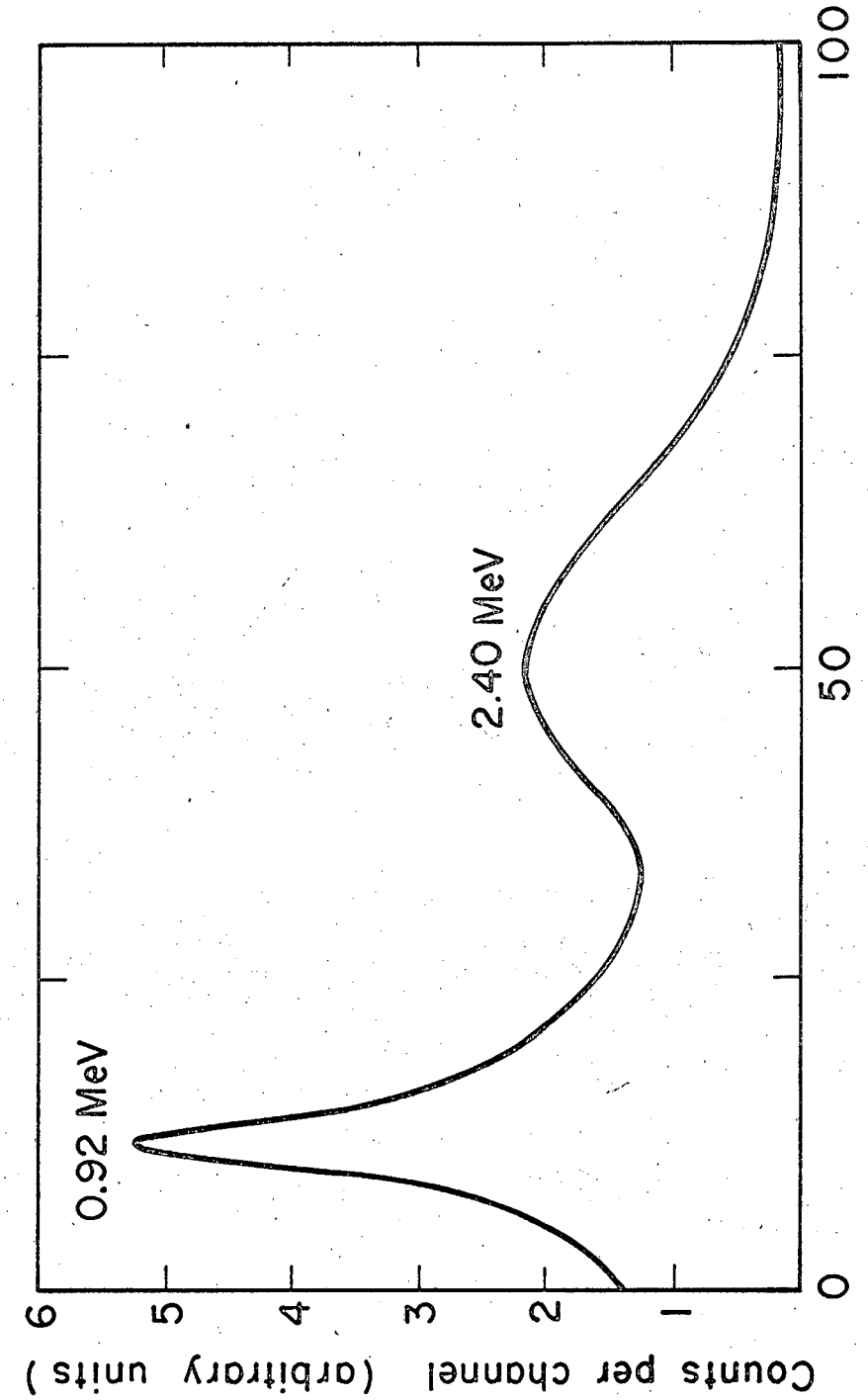

MUB-6095

Fig. 14

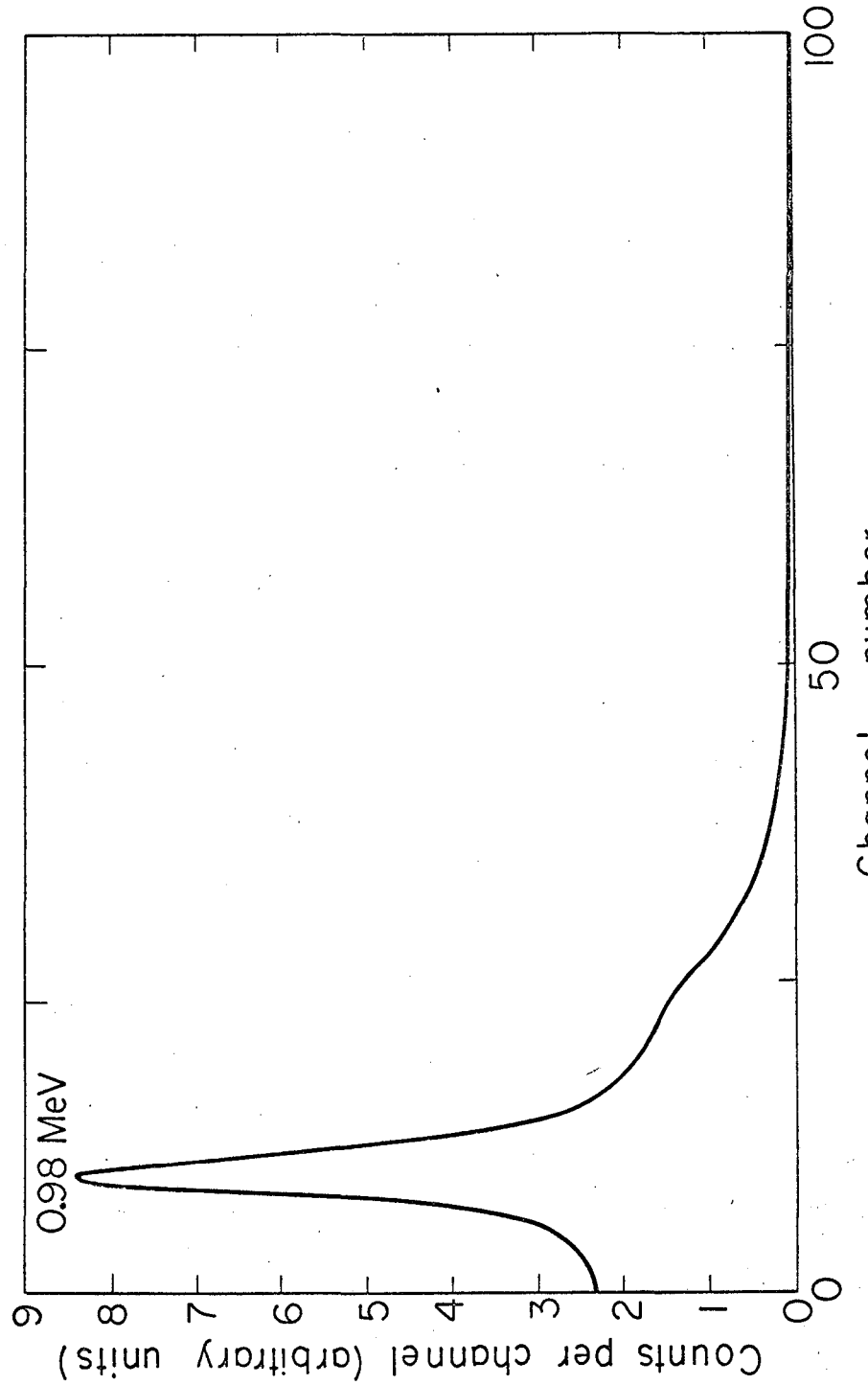

MUB-6090

Fig. 15

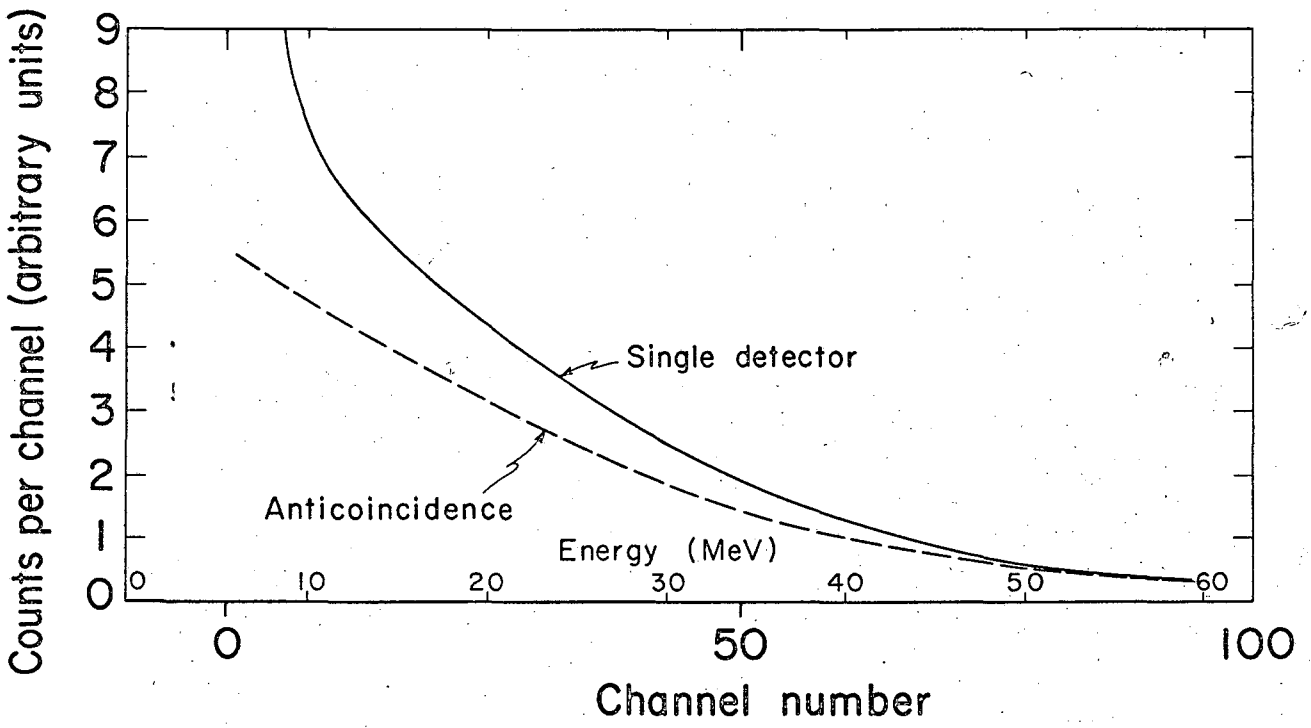
Counts per channel (arbitrary units)
0
1
2
3
4
5
6
7
8
9
Single detector
Anticoincidence
Energy (MeV)
0
10
20
30
40
50
60
0
50
100
Channel number
MUB-4139

Fig. 16